

Article

The Origin of Carbonate Components in Carbonate Hosted Pb-Zn Deposit in the Sichuan-Yunnan-Guizhou Pb-Zn Metallogenic Province and Southwest China: Take Lekai Pb-Zn Deposit as an Example

Zhiwei He ¹, Bo Li ^{2,*} , Xinfu Wang ², Xianguo Xiao ³, Xin Wan ² and Qingxi Wei ⁴¹ College of Earth Science, Chengdu University of Technology, Chengdu 610000, China² Faculty of Land and Resource Engineering, Kunming University of Science and Technology, Kunming 650093, China³ Non-Ferrous Metals and Nuclear Industry Geological Exploration Bureau of Guizhou, Guiyang 550000, China⁴ Kunming Prospecting Design Institute of China Nonferrous Metals Industry Co., Ltd., Kunming 650051, China

* Correspondence: libo8105@kust.edu.cn

Abstract: The Lekai lead–zinc (Pb–Zn) deposit is located in the northwest of the Sichuan–Yunnan–Guizhou (SYG) Pb–Zn metallogenic province, southwest China. Even now, the source of the metallogenic fluid of Pb–Zn deposits in the SYG Pb–Zn metallogenic province has not been recognized. Based on traditional lithography, rare earth elements (REEs), and carbon–oxygen (C–O) isotopes, this work uses the magnesium (Mg) isotopes of hydrothermal carbonate to discuss the fluid source of the Lekai Pb–Zn deposit and discusses the fractionation mechanism of Mg isotopes during Pb–Zn mineralization. The REE distribution patterns of hydrothermal calcite/dolomite are similar to that of Devonian sedimentary carbonate rocks, which are all present steep right-dip type, indicating that sedimentary carbonate rocks may be serve as the main source units of ore-forming fluids. The C–O isotopic results of hydrothermal dolomite/calcite and the $\delta^{13}\text{C}_{\text{PDB}}-\delta^{18}\text{O}_{\text{SMOW}}$ diagram show that dolomite formation is closely related to the dissolution of marine carbonate rocks, and calcite may be affected to some extent by basement fluid. The Mg isotopic composition of dolomite/calcite ranges from -3.853% to -1.358% , which is obviously lighter than that of chondrites, mantle, or seawater and close to that of sedimentary carbonate rock. It shows that the source of the Mg element in metallogenic fluid of Lekai Pb–Zn deposit may be sedimentary carbonate rock rather than mantle, chondrites, or seawater. In addition, the mineral phase controls the Mg isotope fractionation of dolomite/calcite in the Lekai Pb–Zn deposit. Based on the geological, mineralogical, and hydrothermal calcite/dolomite REE, C–O isotope, and Mg isotope values, this work holds that the mineralization of the Lekai Pb–Zn deposit is mainly caused by basin fluids, influenced by the basement fluids; the participation of basement fluids affects the scale and grade of the deposit.

Keywords: Sichuan–Yunnan–Guizhou Pb–Zn metallogenic province; Lekai Pb–Zn deposit; calcite/dolomite REE; C–O–Mg isotope; metallogenic fluid source



Citation: He, Z.; Li, B.; Wang, X.; Xiao, X.; Wan, X.; Wei, Q. The Origin of Carbonate Components in Carbonate Hosted Pb–Zn Deposit in the Sichuan–Yunnan–Guizhou Pb–Zn Metallogenic Province and Southwest China: Take Lekai Pb–Zn Deposit as an Example. *Minerals* **2022**, *12*, 1615. <https://doi.org/10.3390/min12121615>

Academic Editor: Maria Boni

Received: 14 November 2022

Accepted: 13 December 2022

Published: 15 December 2022

Publisher's Note: MDPI stays neutral with regard to jurisdictional claims in published maps and institutional affiliations.



Copyright: © 2022 by the authors. Licensee MDPI, Basel, Switzerland. This article is an open access article distributed under the terms and conditions of the Creative Commons Attribution (CC BY) license (<https://creativecommons.org/licenses/by/4.0/>).

1. Introduction

Located in the southwest margin of Yangtze Block, the Sichuan–Yunnan–Guizhou (SYG) Pb–Zn metallogenic province is one of the main production bases of Pb–Zn–Ag–Ge and other metal elements in China and also an important part of the giant south China Mesozoic low-temperature metallogenic domain [1]. The Pb–Zn deposits in this region are mainly hosted in Sinian to Permian carbonates, which are obviously controlled by the fracture and generally present the characteristics of one orebody occurring in multiple strata. The northeast Yunnan metallogenic belt in the metallogenic province is mainly controlled by the northeast (NE)–trending tectonic belt, producing the super large Pb–Zn deposits

(i.e., Huize and Lemachang) and large Pb-Zn deposits (i.e., Maozu and Maoping) [2,3]. Sinian, Cambrian, Devonian, and Carboniferous are the main ore host sequences for the Pb-Zn orebodies in northeast Yunnan. The metallogenic belt in northwestern Guizhou is mainly controlled by the northwest (NW)–trending tectonic belt, producing one super large Pb-Zn deposit (i.e., Zhugongtang) and a large number of small to medium-sized Pb-Zn deposits. Carboniferous and Permian are the main ore host sequences for the Pb-Zn orebodies in northwestern Guizhou. Compared with the northeast Yunnan metallogenic belt, the ore host sequences of the northwestern Guizhou metallogenic belt are relatively newer, the deposit scale is smaller, the average grade is lower, and the types of Ag–Ge–Cd–In–Ga and other metal elements are fewer. The Lekai Pb-Zn deposit is located in the northwest Guizhou metallogenic belt, but it has a similar metallogenic geological setting to the northeast Yunnan metallogenic belt (Figure 1). This study of the Lekai Pb-Zn deposit is conducive to the comparative study of metallogenic materials and fluid sources of the northwest Guizhou and northeast Yunnan metallogenic belts.

Recently, a variety of geochemical methods have been widely used to determine the properties and sources of ore-forming fluid in the SYG Pb-Zn metallogenic province, including the petrography of fluid inclusions in quartz, calcite, and sphalerite [2,4]; H–O–Sr isotopic composition of calcite [5,6]; C–O isotope and rare earth element (REE) analysis of calcite; and S–Pb isotope analysis of sulfides [1,7–10]. Concurrently, accompanied by the development of high-precision testing instruments, such as NanoSIMS and laser ablation inductively coupled plasma mass spectroscopy, the application of microscale in situ testing technology tends to be mature, such as the measurement of sulfide in situ trace elements and S–Pb isotopes, which greatly improves the testing accuracy [5,11,12]. At present, the nontraditional stable isotope geochemistry of Fe, Cu, Zn, Cd, and Mg has made great progress and shown great application potential in tracing the source of ore-forming materials [13–19]. In particular, the Zn–Cd isotopes of sphalerite provide more direct evidence for the source of metal elements in Pb-Zn deposits [16,20,21]. However, there is no consensus on the contributions of sedimentary rocks, basement rocks, or magmatic rocks to metallogenic materials.

The information contained in hydrothermal carbonate rocks can well reflect the source and physicochemical characteristics of metallogenic fluids, and this information has been widely used in research on ore deposits. Mg is the core element of hydrothermal carbonate rocks, and isotopic testing technology (multicollector-inductively coupled plasma mass spectroscopy [MC–ICP–MS]) has led to the establishment of the isotope geochemical system [22–26], which has gradually become a new means to study carbonate rocks. Mg isotope has unique advantages in revealing the process of epigenetic geological processes, dolomite genesis, crust–mantle material circulation, and the exploration of fluid properties and sources of low-temperature deposits [27–29].

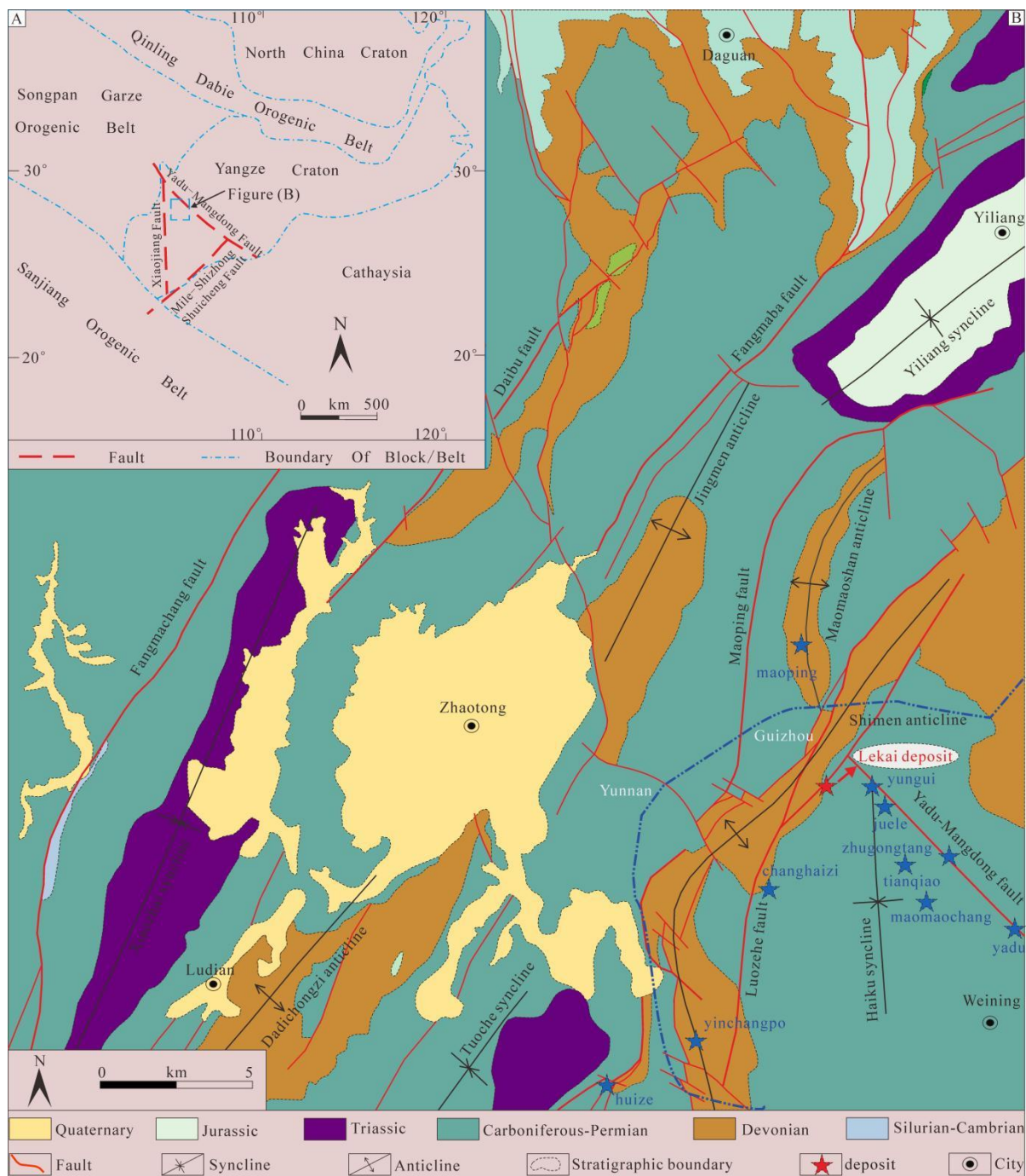


Figure 1. (A) Regional geological framework of south China [7]; (B) Regional geological map of Lekai Pb-Zn deposit in SYG Pb-Zn metallogenic province [30].

The Mg isotopic composition of main reservoirs and the mechanism of Mg isotopic behavior in geological processes provide a theoretical basis for the tracing of metallogenic fluids. At present, there has been a certain degree of data accumulation in the study of Mg isotopes [13–15,23,25,29,31–39]. These data have revealed that the Earth’s materials, mantle peridotites, and basalts were relatively heavy Mg isotopic compositions (peridotites had $\delta^{26}\text{Mg}$ values ranging from -0.48‰ to 0.06‰ , average: $-0.23 \pm 0.19\text{‰}$; basalts had $\delta^{26}\text{Mg}$ values ranging from -0.09‰ to 0.46‰ , average: $-0.24 \pm 0.12\text{‰}$), which are relatively homogeneous and similar to those of chondrites ($\delta^{26}\text{Mg}$ values ranging from -0.35‰ to -0.20‰ , average: $-0.28 \pm 0.06\text{‰}$) [23,34]. Compared with mantle rocks, the Mg isotopic

composition of seawater is relatively light but also relatively homogeneous ($\delta^{26}\text{Mg}$ values range from -0.87‰ to -0.75‰ , average: $-0.83 \pm 0.07\text{‰}$) [23,33,34]. The Mg isotopic composition of carbonate rocks is the lightest, and its variation is the largest ($\delta^{26}\text{Mg} = -4.84\text{‰}$ to -1.00‰ , average: $-3.09 \pm 2.66\text{‰}$) [14,23,36–38]. The $\delta^{26}\text{Mg}$ values of dolomite and limestone range from -2.29‰ to -1.09‰ and -4.47‰ to -2.43‰ , respectively [29,31–39]. The $\delta^{26}\text{Mg}$ values of sedimentary rocks (excluding carbonate rocks) mainly range from -0.94‰ to 0.92‰ , with an average of $-0.06 \pm 0.60\text{‰}$ [25]. Therefore, there are significant differences in the Mg isotopic composition and distribution range among each of Earth's reservoirs. In particular, the greatest differences in Mg isotopic composition are between mantle and sedimentary rocks. This is the important basis of Mg isotopes in tracing the source of metallogenic materials and restricting mineralization.

This study selects the hydrothermal carbonate minerals (i.e., dolomite and calcite) of the Lekai Pb-Zn deposit as the main objects, which are based on systematic petrography and geology. Detailed REE and C–O isotopic compositions of dolomite and calcite were studied. The Mg isotopic data of hydrothermal carbonate rocks are experimentally measured, and the REE, C, O, and Mg isotopic compositions of hydrothermal carbonate rocks in the deposit are comprehensively analyzed using these data. The REE and C, O, and Mg isotopic compositions of the hydrothermal carbonate rocks in the Lekai Pb-Zn deposit are analyzed. The sources of metallogenic material and fractionation factors of Mg isotopes in the mineralization process of the Lekai Pb-Zn deposit are identified.

2. Geological Background and Deposit Geology

The Yangtze Block is mainly composed of basement metamorphic rocks, marine/continental sedimentary rocks, and igneous rocks. The basement metamorphic rocks are a set of dioritic, granitic mixed gneiss, migmatitic, and other deep metamorphic rocks of the Paleoproterozoic Kangding group and a set of shallow to medium metamorphic rocks of the Mesoproterozoic Kunyang/Huili Formation. The caprock sequence is mainly composed of Sinian to Permian marine facies and Mesozoic to Cenozoic continental sedimentary rocks. The igneous rocks are mainly dominated by the Emeishan basalt and homologous diabase in the Late Permian [12,40]. The tectonic deformation of the Yangtze Block is dominated by deep faults and folds. It has experienced the Hercynian, Indosinian, and Yanshanian geological evolution stages and was affected by the Himalayan orogeny events. These tectonic events mainly controlled the sedimentation, magmatism, and mineralization in this region [9,38,41]. The Lekai Pb-Zn deposit is mainly controlled by a series of faults and folds formed by the late Indosinian tectonic event.

The Lekai Pb-Zn deposit is the southern extension of the Huize–Yiniang–Niujiie oblique strike-slip fault–fold belt in the northeast Yunnan metallogenic belt and controlled by the NE-trending Luozehe fault–fold belt (Figure 1). The folds mainly developed in the NE-trending Shimen anticline and a series of secondary folds. The broken parts of the secondary folds on the SE wing of Shimen anticline are favorable for mineralization. The faults are mainly presented in the NE- and NW -trending, with “ ξ -type” (xi-type) and “ λ -type” (lambda-type) structural styles. The NE-trending faults are closely related to mineralization and control the distribution of orebodies. The NW- trending faults are smaller in scale and are post-mineralization faults (Figure 2). The Pb-Zn orebodies present layered, stratoid, and lenticular shapes and occur in the folds and faults intersections within the coarse-grained and altered dolomite in the Devonian Wangchengpo formation (D_3w). There are four Pb-Zn orebodies (mineralized bodies) have been identified, which all show the obvious characteristics of slow widening, fast narrowing, expansion, and contraction in plane and section views (Figures 3 and 4A). The Lekai deposit mainly experienced the following two metallogenic formation periods: a hydrothermal metallogenic period and a supergene oxidation period. Ore minerals (i.e., sphalerite, galena, and pyrite and gangue minerals (i.e., dolomite and calcite) are mainly developed in the hydrothermal mineralization period. Ore structures consist of brecciated (Figure 4B), veined (Figure 4C,D), and disseminated (Figure 4D–F) types, and textures consist of hypidiomorphic-idiomorphic grain (Figure 5A),

metasomatic (Figure 5B,C), codissolved (Figure 5E), interstitial (Figure 5D,F), and crushed (Figure 5F) morphologies. The hydrothermal mineralization period can be divided into the following three stages: (i) pyrite + dolomite + sphalerite; (ii) galena + pyrite + sphalerite + calcite; (iii) galena + pyrite. Cerusite, smithsonite, and limonite are the main minerals in the supergene oxidation period (Figure 6).

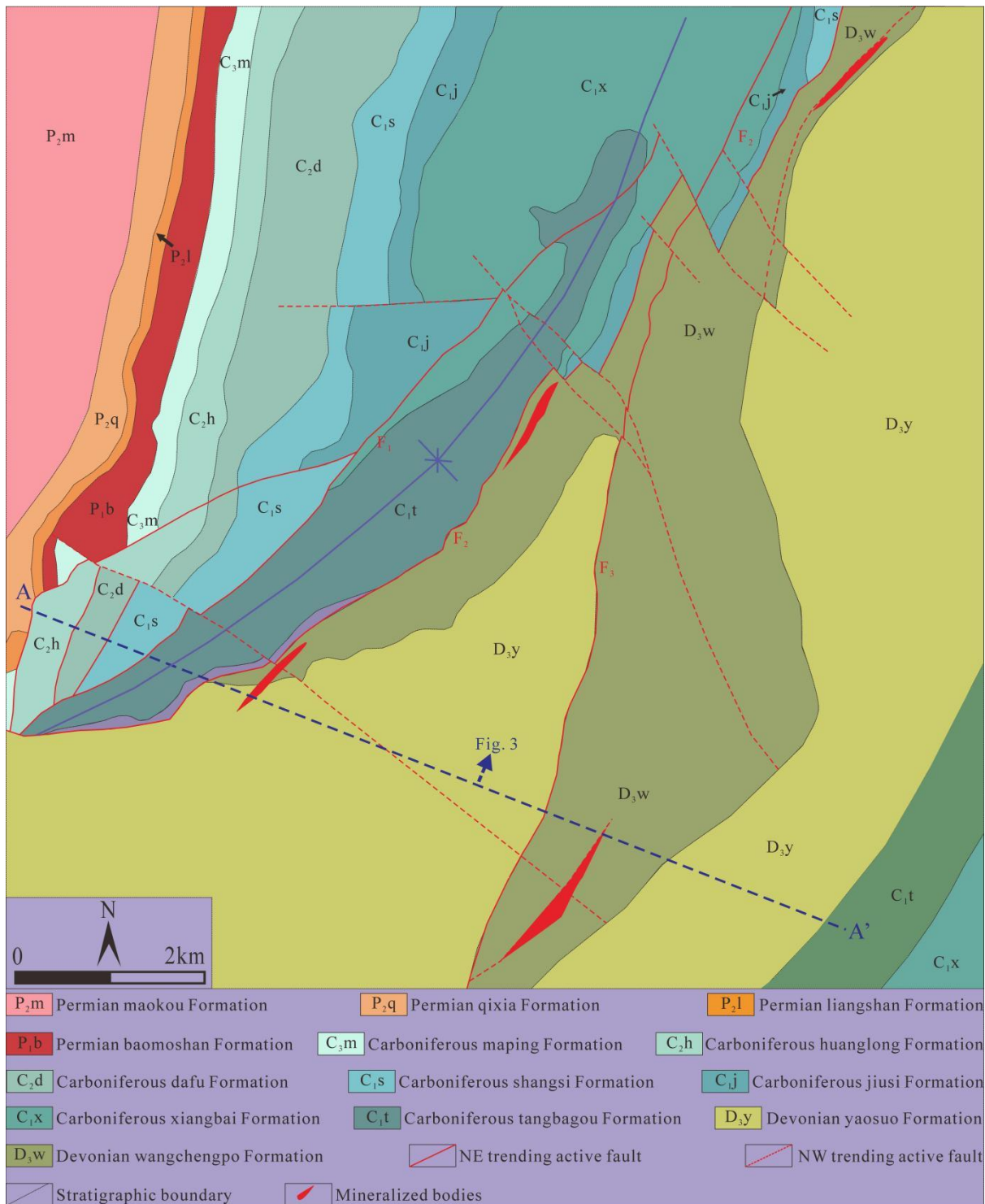


Figure 2. Geological map of Lekai Pb-Zn deposit in SYG Pb-Zn metallogenic province [42].

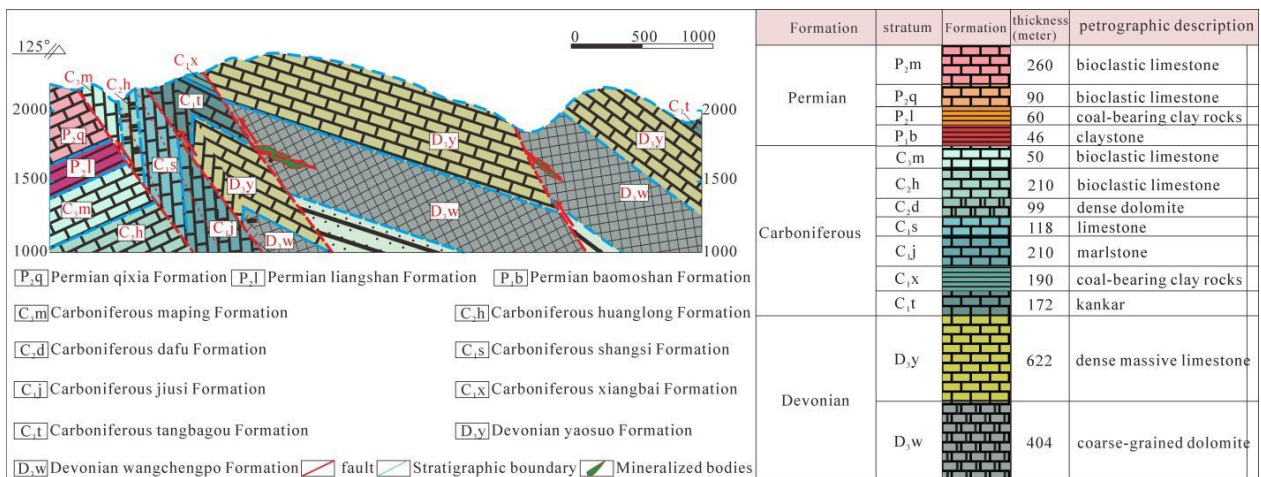


Figure 3. Cross-section map of Lekai Pb-Zn deposit in SYG Pb-Zn metallogenic province [30].

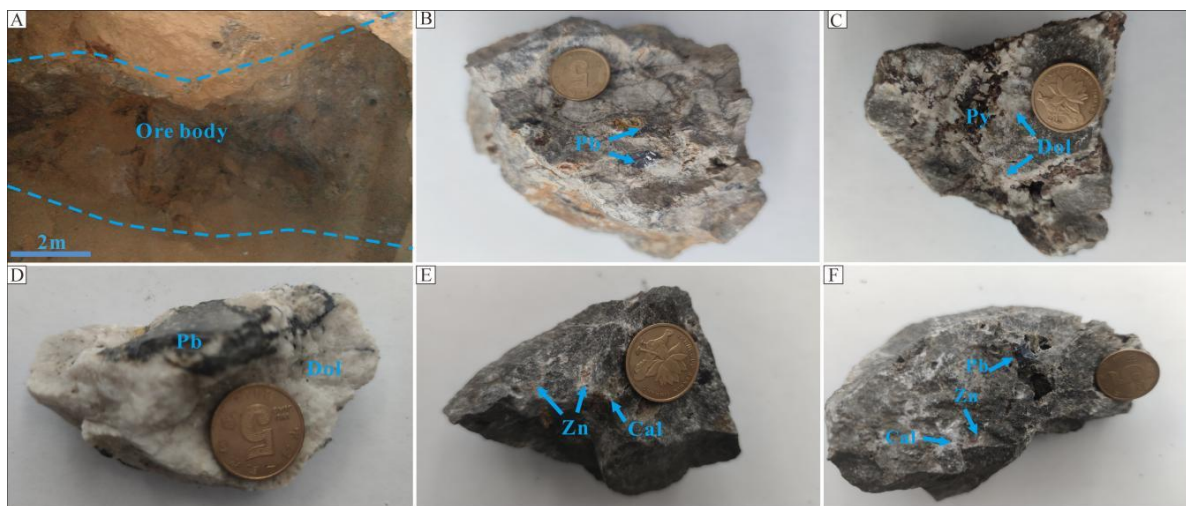


Figure 4. The Pb-Zn orebody and ore structure of Lekai Pb-Zn deposit. (A) Stratoid Pb-Zn orebodies occur within interlayer fracture zone; (B) Brecciated Pb-Zn ore, Galena occurs in brecciated dolomite as an agglomerate; (C) Disseminated Pb-Zn ore, Veined dolomite and pyrite occur in altered dolomite; (D) Cloddy Pb-Zn ore, Agglomerate and veined galena occur in dolomite; (E) Disseminated Pb-Zn ore, Agglomerate sphalerite and calcite occur in dolomite; (F) Cloddy Pb-Zn ore, Sphalerite, galena, and calcite are filled within the dolomite pores. Sp = sphalerite; Py = pyrite; Gn = galena; Cal = calcite; Dol = dolomite.

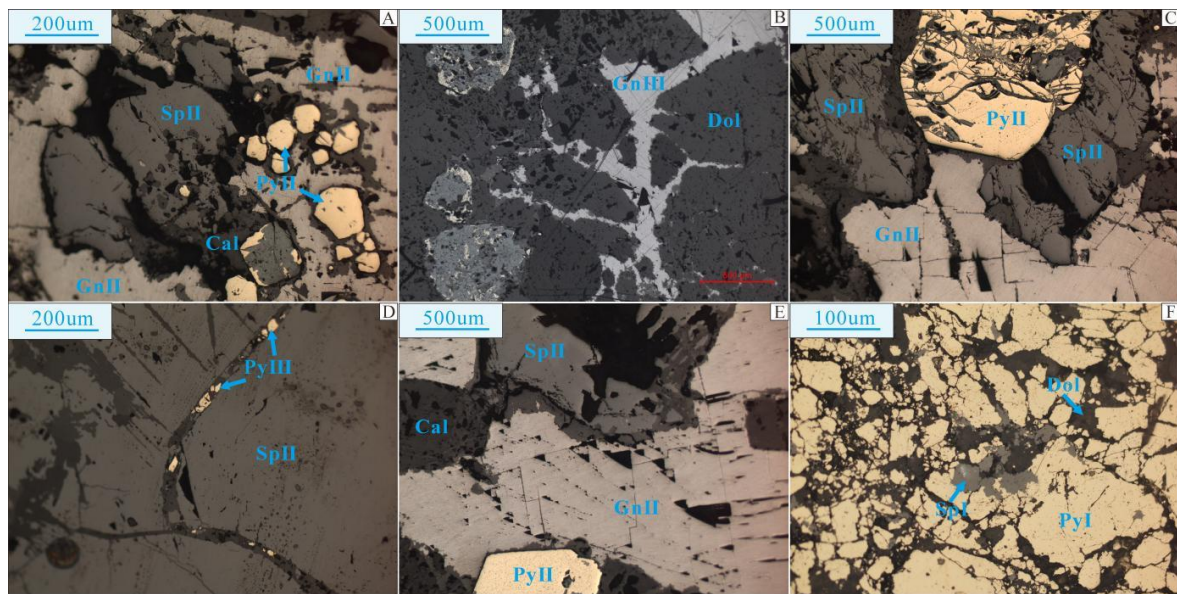


Figure 5. Mineral assemblages and sequence of Lekai Pb-Zn deposit. (A) Sphalerite, galena, and pyrite are hypidiomorphic-idiomorphic grain; Pyrite is surrounded by calcite, sphalerite, and galena form codissolved texture; (B) Veined galena metasomatized dolomite; (C) Sphalerite, galena, and pyrite are granularly cemented by calcite; (D) The later granular pyrite developed in veined calcite and metasomatized earlier formed sphalerite; (E) Pyrite, sphalerite, and galena show a codissolved texture; (F) A small amount of sphalerite is filled within the fracture zones of crushed pyrite. Sp = sphalerite; Py = pyrite; Gn = galena; Cal = calcite; Dol = dolomite.

| Lekai deposit | | | | |
|---------------------|-----------------------------------|--------------|-----------|-----------------|
| Metallogenic stages | Hydrothermal mineralization Stage | | | Supergene Stage |
| Stages | i | ii | iii | |
| Mineral assemblage | Py+Dol | Sp+Gn+Py+Cal | Gn+Py+Cal | |
| Pyrite | More | Less | Less | |
| Sphalerite | Less | More | Less | |
| Galena | | More | Less | |
| Calcite | | More | Less | |
| Dolomite | More | Less | | |
| Limonite | | | | More |
| Cerussite | | | | More |
| Smithsonite | | | | More |

More
 Less

Figure 6. Mineral paragenesis of the Lekai Pb-Zn deposit [30].

3. Sampling and Methods

The samples were mainly collected from adit LD11 of the Lekai Pb-Zn deposit. We take the method of continuous block in adit for sampling. The top and bottom segment of the Pb-Zn orebody is in contact with the altered dolomite, which is mainly disseminated ore, and the center of the orebody is brecciated and cloddy ore. The representative and fresh hydrothermal carbonate samples were collected based on the field’s detailed geological cataloging and observations. Firstly, the samples were crushed to 40–60 mesh. Hydrothermal calcite and dolomite with purities greater than 99% were selected under the binocular microscope, after which the samples were ultrasonically cleaned and repeatedly purified. The pure single-grain samples were pounded to 200 mesh with an agate mortar for REE, C, O, and Mg isotope analyses. REE and C–O isotope analyses were performed at the State

Key Laboratory of Ore Deposit Geochemistry, Institute of Geochemistry, Chinese Academy Sciences, and Mg isotope analyses were undertaken at Aoshi analytical testing Co., Ltd, Guangzhou, China.

The REE contents of the calcite/dolomite samples were measured via inductively coupled plasma mass spectroscopy (ICP-MS; ELAN DRC-e four-stage bar inductively coupled plasma mass spectrometer; PerkinElmer, Woodbridge, ON, Canada); the analysis uncertainty was less than 5%. Bulk C–O isotope analyses were conducted using a Finnigan MAT-253 mass spectrometer (Thermo Fisher Scientific, Waltham, MA, USA). Calcite/dolomite samples were reacted with 100% H₃PO₄ to produce CO₂. The analytical precision rates calculated from replicate analyses of unknown samples were better than 0.2‰ (2σ) and 1‰ (2σ) for δ¹³C and δ¹⁸O, respectively. The δ¹³C and δ¹⁸O values were reported relative to the Vienna Pee Dee Belemnite (V-PDB) standard and Standard Mean Ocean Water (SMOW), respectively.

Hydrothermal calcite/dolomite samples were prepared via alkali fusion and digestion using acids, followed by separation of Mg via ion exchange AG 50W-8X (Bio-Rad, Hercules, CA, USA) and measurement via MC-ICP-MS (NEPTUNE PLUS) (Thermo Fisher Scientific, Shanghai, China) for Mg isotopes (ratio). Si was added to all analytical solutions (purified Mg fractions, standards, and blanks) as a spike internal standard to correct mass bias and ensure the best precision of Mg isotope values. Delta values for Mg were calculated against IRMM-3704 CRM.

4. Results

4.1. REE Contents

Hydrothermal calcite/dolomite is characterized by an increase in total REE (excluding Y, ΣREE) concentrations from 2.45 to 29.11 ppm, with an average of 6.05 ppm ($n = 13$) (Table 1, Figure 7A,B). The concentrations of light (LREEs) and heavy REEs (HREEs) range from 2.02 to 25.02 ppm (average: 5.18 ppm, $n = 13$) and 0.31 to 4.09 ppm (average: 0.87 ppm, $n = 13$), respectively. The LREE/HREE ratios of calcite/dolomite samples were between 4.33 and 8.06 (average: 5.93, $n = 13$); the (La/Yb)_N values range from 6.17 to 13.32 and showed LREE enrichment patterns. The differences between LREE and HREE concentrations were obvious, and the chondrite-normalized REE patterns were consistently steep right-sloping types (Figure 7A). The Eu and Ce show moderate negative anomalies, with δEu and δCe values ranging from 0.56 to 0.69 and 0.63 to 0.87, respectively.

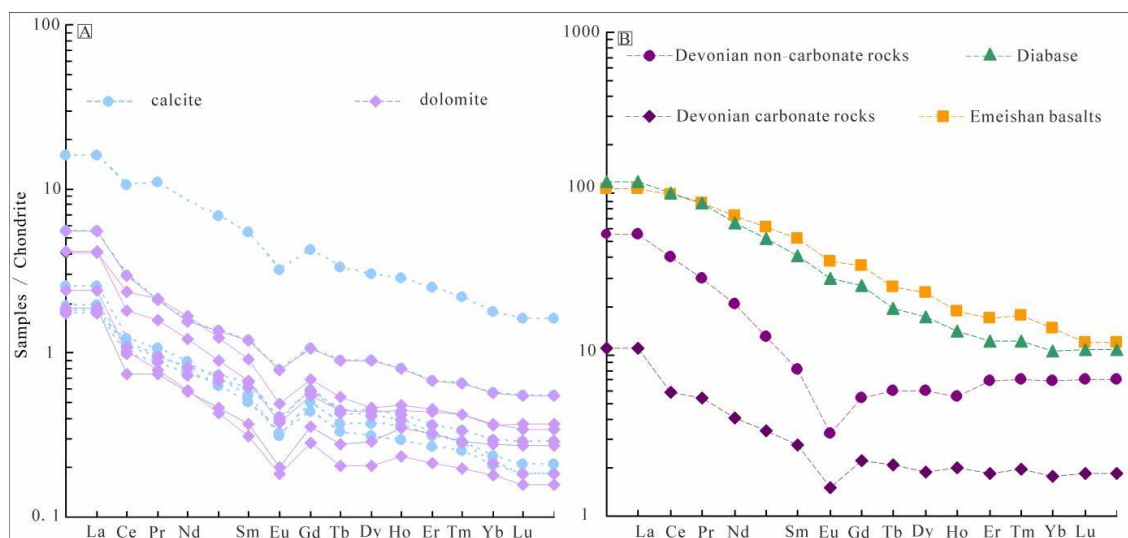


Figure 7. (A) The rare earth elements distribution of calcite and dolomite in Lekai Pb-Zn deposits; (B) The rare earth elements distribution of carbonate rocks and non-carbonate rocks in Devonian, Emeishan basalts, and Diabase in SYG Pb-Zn metallogenic province [43].

Table 1. Analysis results of REE contents of hydrothermal calcite/dolomite samples from the Lekai Pb-Zn deposit.

| Sample Minerals | LK635 | LK600 | LD01R24 LD01R3 LD01R2 LD01R1 | | | | Average | LK122-3 | LK122 | LD03R8 LD03R6 LD01R3 LD01R2 LD01R1 | | | | Average | |
|----------------------------------|-------|-------|------------------------------|-------|-------|-------|---------|---------|-------|------------------------------------|-------|-------|-------|---------|-------|
| | | | Calcite (ppm) | | | | | | | Dolomite (ppm) | | | | | |
| La | 0.72 | 5.89 | 0.93 | 0.64 | 0.67 | 2.04 | 1.82 | 1.51 | 1.54 | 0.89 | 0.69 | 0.86 | 0.93 | 1.47 | 1.13 |
| Ce | 1.09 | 10.10 | 1.17 | 0.95 | 1.03 | 2.85 | 2.87 | 2.24 | 1.73 | 0.98 | 0.71 | 0.97 | 1.01 | 2.01 | 1.38 |
| Pr | 0.13 | 1.49 | 0.15 | 0.12 | 0.13 | 0.29 | 0.39 | 0.29 | 0.22 | 0.11 | 0.10 | 0.14 | 0.14 | 0.28 | 0.18 |
| Nd | 0.56 | 6.00 | 0.62 | 0.52 | 0.58 | 1.11 | 1.57 | 1.20 | 0.86 | 0.42 | 0.42 | 0.56 | 0.55 | 1.11 | 0.73 |
| Sm | 0.12 | 1.26 | 0.13 | 0.14 | 0.15 | 0.28 | 0.35 | 0.21 | 0.16 | 0.07 | 0.09 | 0.12 | 0.11 | 0.21 | 0.14 |
| Eu | 0.03 | 0.28 | 0.03 | 0.04 | 0.03 | 0.07 | 0.08 | 0.04 | 0.03 | 0.02 | 0.02 | 0.03 | 0.02 | 0.05 | 0.03 |
| Gd | 0.13 | 1.30 | 0.15 | 0.18 | 0.18 | 0.33 | 0.38 | 0.21 | 0.17 | 0.09 | 0.11 | 0.14 | 0.13 | 0.23 | 0.15 |
| Tb | 0.02 | 0.19 | 0.02 | 0.03 | 0.03 | 0.05 | 0.06 | 0.03 | 0.03 | 0.01 | 0.02 | 0.02 | 0.02 | 0.04 | 0.02 |
| Dy | 0.12 | 1.16 | 0.14 | 0.16 | 0.17 | 0.34 | 0.35 | 0.18 | 0.17 | 0.08 | 0.11 | 0.14 | 0.14 | 0.23 | 0.15 |
| Ho | 0.03 | 0.24 | 0.03 | 0.03 | 0.04 | 0.07 | 0.07 | 0.04 | 0.04 | 0.02 | 0.03 | 0.03 | 0.03 | 0.05 | 0.03 |
| Er | 0.07 | 0.62 | 0.08 | 0.08 | 0.09 | 0.17 | 0.19 | 0.11 | 0.11 | 0.05 | 0.08 | 0.09 | 0.09 | 0.15 | 0.1 |
| Tm | 0.01 | 0.08 | 0.01 | 0.01 | 0.01 | 0.02 | 0.02 | 0.02 | 0.02 | 0.01 | 0.01 | 0.01 | 0.01 | 0.02 | 0.01 |
| Yb | 0.05 | 0.44 | 0.06 | 0.05 | 0.07 | 0.14 | 0.14 | 0.09 | 0.09 | 0.05 | 0.07 | 0.08 | 0.07 | 0.13 | 0.08 |
| Lu | 0.01 | 0.06 | 0.01 | 0.01 | 0.01 | 0.02 | 0.02 | 0.01 | 0.01 | 0.01 | 0.01 | 0.01 | 0.01 | 0.02 | 0.01 |
| Y | 1.51 | 9.31 | 2.02 | 1.90 | 1.95 | 3.36 | 3.34 | 2.41 | 2.25 | 1.26 | 1.96 | 2.01 | 1.97 | 2.66 | 2.07 |
| ΣREE | 3.08 | 29.11 | 3.52 | 2.95 | 3.19 | 7.78 | 8.27 | 6.19 | 5.16 | 2.79 | 2.45 | 3.18 | 3.26 | 5.99 | 4.15 |
| LREE | 2.65 | 25.02 | 3.02 | 2.41 | 2.59 | 6.64 | 7.06 | 5.50 | 4.53 | 2.48 | 2.02 | 2.66 | 2.75 | 5.12 | 3.58 |
| HREE | 0.43 | 4.09 | 0.50 | 0.55 | 0.60 | 1.14 | 1.22 | 0.69 | 0.63 | 0.31 | 0.44 | 0.52 | 0.51 | 0.87 | 0.57 |
| LREE/HREE | 6.15 | 6.12 | 6.05 | 4.40 | 4.33 | 5.80 | 5.48 | 7.93 | 7.22 | 8.06 | 4.64 | 5.12 | 5.40 | 5.87 | 6.32 |
| La _N /Yb _N | 9.49 | 9.07 | 10.92 | 8.12 | 6.17 | 9.71 | 8.91 | 11.34 | 11.31 | 13.32 | 6.73 | 7.55 | 8.56 | 7.64 | 9.49 |
| δEu | 0.69 | 0.66 | 0.60 | 0.67 | 0.63 | 0.69 | 0.66 | 0.62 | 0.62 | 0.62 | 0.56 | 0.61 | 0.62 | 0.67 | 0.62 |
| δCe | 0.82 | 0.80 | 0.74 | 0.80 | 0.82 | 0.87 | 0.81 | 0.79 | 0.70 | 0.74 | 0.63 | 0.67 | 0.67 | 0.74 | 0.71 |
| Y/Ho | 60.4 | 38.63 | 66.30 | 57.58 | 54.17 | 49.41 | 54.42 | 58.78 | 59.21 | 63.00 | 66.5 | 64.84 | 61.56 | 50.19 | 60.58 |
| La/Ho | 28.64 | 24.44 | 30.52 | 19.30 | 18.50 | 30.00 | 25.23 | 36.83 | 40.53 | 44.35 | 23.40 | 27.74 | 28.91 | 27.74 | 32.78 |
| Tb/La | 0.03 | 0.03 | 0.02 | 0.04 | 0.04 | 0.03 | 0.03 | 0.02 | 0.02 | 0.01 | 0.02 | 0.02 | 0.02 | 0.02 | 0.02 |
| Sm/Nd | 0.20 | 0.21 | 0.20 | 0.28 | 0.26 | 0.25 | 0.23 | 0.18 | 0.18 | 0.17 | 0.20 | 0.21 | 0.19 | 0.19 | 0.19 |

4.2. C and O Isotopes

The C and O isotopic compositions of calcite/dolomite samples separated from the sulfide ore are listed in Table 2. The δ¹³C_{PDB} and δ¹⁸O_{SMOW} values of calcite ranging from −6.02‰ to 2.40‰ (average: −3.26‰, n = 6) and 14.72‰ to 20.14‰ (average: 16.19‰, n = 6), respectively. The δ¹³C_{PDB} and δ¹⁸O_{SMOW} values of dolomite ranging from −0.33‰ to 2.29‰ (average: 0.93‰, n = 7) and 19.06‰ to 26.16‰ (average: 22.27‰, n = 7), respectively.

Table 2. C-O isotopic composition of hydrothermal calcite/dolomite in Lekai Pb-Zn deposit.

| Sample Number | Mineral | δ ¹³ C (‰V _{PDB}) | Std.ev | δ ¹⁸ O (‰V _{PDB}) | Std.ev | δ ¹⁸ O (‰SMOW) |
|---------------|----------|--|--------|--|--------|---------------------------|
| LD01R1 | Calcite | −3.57 | 0.02 | −14.99 | 0.02 | 15.41 |
| LD01R2 | Calcite | −3.78 | 0.05 | −15.32 | 0.10 | 15.07 |
| LD01R3 | Calcite | −3.59 | 0.04 | −15.66 | 0.03 | 14.72 |
| LD01R24 | Calcite | −5.00 | 0.05 | −13.92 | 0.09 | 16.51 |
| LK600 | Calcite | 2.40 | 0.07 | −10.40 | 0.10 | 20.14 |
| LK635 | Calcite | −6.02 | 0.08 | −15.11 | 0.08 | 15.28 |
| Average | | −3.26 | 0.05 | −14.23 | 0.07 | 16.19 |
| LD01R1 | Dolomite | 0.53 | 0.05 | −9.86 | 0.06 | 20.70 |
| LD01R2 | Dolomite | 1.52 | 0.02 | −6.78 | 0.03 | 23.87 |
| LD01R3 | Dolomite | 1.61 | 0.03 | −8.57 | 0.03 | 22.03 |
| LD03R6 | Dolomite | 1.01 | 0.05 | −8.77 | 0.07 | 21.82 |
| LD03R8 | Dolomite | −0.33 | 0.05 | −11.45 | 0.08 | 19.06 |
| LK122 | Dolomite | 2.29 | 0.04 | −4.56 | 0.03 | 26.16 |
| LK122-3 | Dolomite | −0.11 | 0.02 | −8.34 | 0.03 | 22.26 |
| Average | | 0.93 | 0.04 | −8.33 | 0.05 | 22.27 |

4.3. Mg Isotopes

The Mg isotopic compositions of calcite and dolomite samples are given in Table 3. The δ²⁶Mg values of seven hydrothermal carbonates (calcite and dolomite) range from −3.853‰ to −1.358‰, with an average of −2.433‰. Three calcite and four dolomite samples had δ²⁶Mg values ranging from −3.853‰ to −3.483‰ (average: −3.613‰) and −1.751‰ to −1.358‰ (average: −1.548‰), respectively.

Table 3. Mg isotopic composition of hydrothermal calcite/dolomite in Lekai Pb-Zn deposit.

| Sample Number | Sample Name | $\delta^{25}\text{Mg}$ | Std.ev | $\delta^{26}\text{Mg}$ | Std.ev |
|---------------|-------------|------------------------|--------|------------------------|--------|
| LD01R2 | Calcite | −1.736 | 0.059 | −3.503 | 0.085 |
| LD01R24 | Calcite | −1.905 | 0.061 | −3.853 | 0.078 |
| LK600 | Calcite | −1.746 | 0.071 | −3.483 | 0.093 |
| Average | Calcite | −1.796 | 0.064 | −3.613 | 0.085 |
| LD01R1 | Dolomite | −0.701 | 0.041 | −1.429 | 0.069 |
| LD01R2 | Dolomite | −0.801 | 0.047 | −1.655 | 0.074 |
| LD03R8 | Dolomite | −0.659 | 0.051 | −1.358 | 0.062 |
| LK122 | Dolomite | −0.859 | 0.040 | −1.751 | 0.060 |
| Average | Dolomite | −0.755 | 0.045 | −1.548 | 0.066 |

5. Discussion

5.1. Genetic Relationship of Hydrothermal Carbonate Rocks and the Nature of Fluids

REE geochemistry is a useful tool in investigating hydrothermal mineralization and understanding the genesis of carbonate rocks in different geological environments [42]. Calcite and dolomite are the main carbonate minerals, which were closely associated with galena, pyrite, and sphalerite in the Lekai Pb-Zn deposit. They have similar REE distribution patterns and show consistent ΣREE , Eu, and Ce anomalies, etc.; in addition, they show constant Y/Ho values and are roughly horizontally distributed on the Y/Ho–La/Ho diagram (Figure 8A), indicating that dolomite and calcite may have crystallized at approximately the same period and originated from the same fluid system.

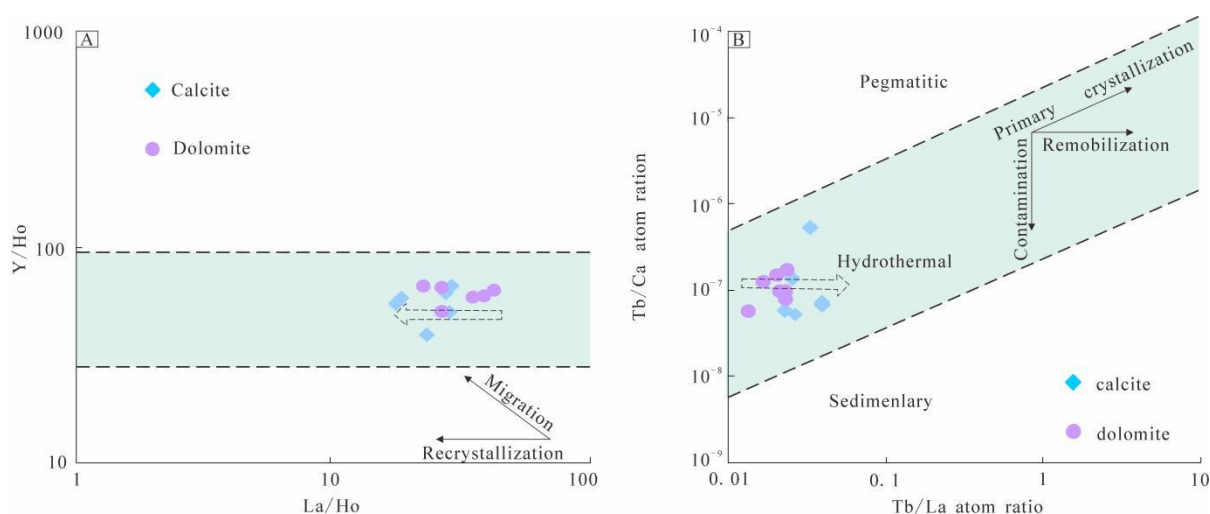


Figure 8. Plots of (A) Y/Ho versus La/Ho ratios and (B) Tb/Ca versus Tb/La ratios for the Lekai calcite and dolomite. (The original base map of A and B after [44,45], respectively).

In fact, there are slight differences in LREE/HREE fractionation between dolomite and calcite, although they both show LREE-enriched patterns with constant LREE/HREE ratios. The average LREE/HREE of dolomite (6.32, $n = 6$) is slightly higher than that of calcite (5.48, $n = 7$). Morgan et al. (1980) believed that the REE pattern in hydrothermal minerals is mainly controlled by the ionic radius of cations and that the LREEs are easier to incorporate into carbonate rock crystal lattices than the HREEs because the differences in ionic radii between LREE^{3+} and Ca^{2+} are smaller than these between HREE^{3+} and Ca^{2+} . Therefore, carbonate rocks should have LREE-enriched patterns as found in this study. LREE/HREE differentiation of hydrothermal carbonates is mainly controlled by physicochemical conditions, which control REE leaching and fluid migration in source rocks [46]. Bau and Möller (1992) [47] suggested that the leaching and fluid migration of REEs may take place in two different states—adsorption and complexation. Specifically,

with the increase of pH value and the decrease of temperature, complexation is more common than adsorption, and a partition mode rich in LREEs is generated in adsorption conditions (such as low pH and high temperature), or ligand-rich fluids can form LREE-poor partition patterns through the complexation process [48–50] because HREEs can form more stable complexes with ligands (CO_3^{2-} and OH^-). Therefore, the fluids in the early stage tend to be rich in LREEs, while HREEs tend to precipitate preferentially in the late stage. We think that dolomite with higher LREE contents may crystallize earlier than calcite. In the process of fluid evolution and carbonate precipitation, not only is there LREE/HREE differentiation, but the Tb/La and Sm/Nd ratios also have differences. Constantopoulos (1988) [50] and Chesley et al. (1991) [51] proposed that the ratios of Tb/La and Sm/Nd of early carbonate rocks are lower than those of late carbonate rocks. The Tb/La ratio of dolomite in the Lekai deposit ranges from 0.01 to 0.02, with an average of 0.02 ($n = 7$), which is slightly lower than that of calcite (0.02–0.04, average: 0.03, $n = 6$); the Sm/Nd ratio of dolomite is between 0.17 and 0.20 (average: 0.19, $n = 7$), which is slightly lower than the Sm/Nd ratio of calcite (0.20–0.28, average: 0.24, $n = 6$). This also supports the view that calcite crystallization may be slightly later than dolomite crystallization.

The dolomite and calcite in the Lekai deposit show moderate negative Eu and Ce anomalies, which indicate that low oxygen fugacity and low-temperature environments occurred during their deposition [52,53]. Considering that there are only a few differences between dolomite and calcite in REE compositions, Tb/La and Sm/Nd ratios, and δEu and δCe values, we preliminarily suspect that they are products of different stages in the evolution of homologous fluids. Dolomite formed earlier and was more influenced by the surrounding rock of Devonian, while calcite formed later, showing more characteristics of the ore-forming fluids.

5.2. Sources of Metallogenic Fluids

5.2.1. REE and C–O Isotopic Constraints

Y and Ho usually show similar geochemical behavior, so the Y/Ho ratio is an important parameter to trace fluid processes [42]. The Y/Ho ratios of hydrothermal dolomite and calcite range from 50.19 to 66.50 and 38.63 to 60.40, respectively, indicating the existence of hydrothermal sources (for which the Y/Ho ratios are approximately 20–110 [44]). The La/Ho ratio of the Devonian surrounding rock (average: 33.79, $n = 2$), dolomite (average: 32.78, $n = 7$), and calcite (average: 25.23, $n = 6$) in the study area gradually decrease, indicating that dolomite and calcite may be hydrothermal carbonates formed by the recrystallization of Devonian rocks in the host rock. Conversely, the REE patterns of dolomite and calcite in the Lekai mining district are consistent with those of Devonian rocks (carbonate and noncarbonate rocks); however, magmatic rocks (Emeishan basalt and diabase) show completely different REE patterns, indicating that dolomite and calcite may have a genetic relationship with the Devonian rocks rather than the Emeishan basalt and diabase. In addition, the Tb/Ca–Tb/La diagram (Figure 8B) established by Möller et al. (1976) [45] can distinguish the relationships among dolomite, calcite, and other calcium-bearing minerals and sedimentary, hydrothermal, and magmatic rocks. In particular, the Tb/Ca ratio may be a good indicator of the formation environment of carbonate rocks [54]. All dolomite and calcite in the Lekai mining district fall into the hydrothermal area, and there are no data within the magmatic area, suggesting their genesis may not be related to the magmatic fluid. The ratios of La/Ho and Tb/La are the criteria for the degree of crystallization differentiation of carbonate rocks [54]. The Y/Ho–La/Ho and Tb/Ca–Tb/La diagrams show the changing trends of La/Ho and Tb/La ratios, which better indicate the crystallization differentiation trends of dolomite and calcite. As expected, dolomite crystallizes earlier than calcite, which may indicate the inheritance from sedimentary Devonian rocks to dolomite and calcite.

The $\delta^{13}\text{C}$ values of dolomite and calcite from the Lekai hydrothermal solution range from -0.33‰ to 2.29‰ (average: 0.93‰ , $n = 7$) and -6.02‰ to 2.40‰ (average: -3.26‰ , $n = 6$), respectively, which are significantly higher than those of organic carbon in sediments ($-30.0\text{‰} < \delta^{13}\text{C}_{\text{PDB}} < -10.0\text{‰}$ [55]), slightly higher than those of mantle-derived

magma ($-8.0\text{‰} < \delta^{13}\text{C}_{\text{PDB}} < -4.0\text{‰}$, [56,57]), and basically corresponding within the range of marine carbonate ($-4.0\text{‰} < \delta^{13}\text{C}_{\text{PDB}} < 4.0\text{‰}$, [58]). It is suggested that the carbon of hydrothermal dolomite and calcite may be derived from marine carbonate rocks. The $\delta^{18}\text{O}_{\text{SMOW}}$ values of hydrothermal dolomite range from 20.60‰ to 26.10‰ (average: 22.60‰, $n = 7$), which are significantly higher than that of the common mantle-derived magma ($6.0\text{‰} < \delta^{18}\text{O}_{\text{SMOW}} < 10.0\text{‰}$, [56,57]), and are completely distributed within the marine carbonate rocks ($20.0\text{‰} < \delta^{18}\text{O}_{\text{SMOW}} < 30.0\text{‰}$, [58]). The $\delta^{18}\text{O}_{\text{SMOW}}$ values of calcite range from 14.30‰ to 20.30‰ (average: 16.10‰, $n = 6$) and are distributed between the common mantle-source magma and marine carbonate rocks and obviously lower than those of marine carbonate rock. Although the dissolution of carbonate rocks will lead to almost constant $\delta^{13}\text{C}$ values and reduced $\delta^{18}\text{O}$ values [59], the $\delta^{18}\text{O}_{\text{SMOW}}$ value of dolomite does not change significantly, which suggests that the oxygen isotopes of dolomite may be inherited from marine carbonate rocks, whereas the oxygen isotopes of calcite may be influenced by other fluids.

The $\delta^{13}\text{C}_{\text{PDB}}-\delta^{18}\text{O}_{\text{SMOW}}$ diagram (Figure 9A) shows that the C–O isotopic composition of dolomite and calcite have obvious differences. The C–O isotopic values decrease from dolomite to calcite, suggesting that calcite may crystallize later than dolomite. Calcite is obviously affected by other fluids and does not retain the characteristics of marine carbonate rocks as dolomite does, which is consistent with the REE analyses. Studies have found that the mineralization of Pb–Zn deposits in northwest Guizhou is a mixture of two kinds of fluids, namely fluid rich in metal elements that originated from the basement and fluid rich in sulfate that originated from the stratum [60]. Therefore, we primarily think the basement fluid is the main factor affecting the O isotopic values of hydrothermal calcite.

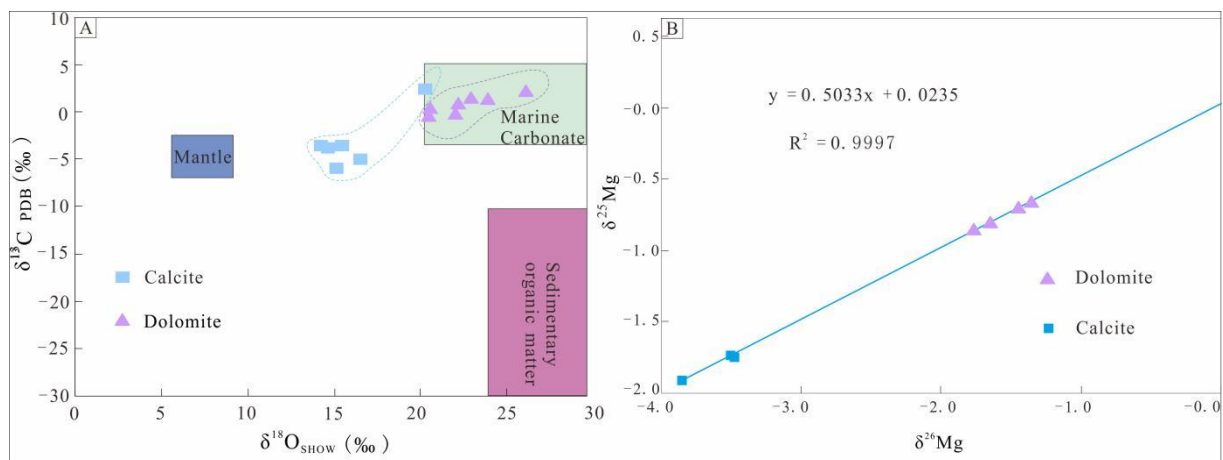


Figure 9. (A) Diagram of $\delta^{13}\text{C}$ vs. $\delta^{18}\text{O}$ of calcite and dolomite in Lekai Pb–Zn deposit (Mantle [56]; Marine Carbonate rocks [58]; Sedimentary organic matters [57]); (B) Diagram of $\delta^{26}\text{Mg}$ vs. $\delta^{25}\text{Mg}$ of calcite and dolomite in Lekai Pb–Zn deposit.

5.2.2. Mg Isotopic Constraints

The Mg isotopic measurements of the Lekai Pb–Zn deposit are all located on the mass fractionation line with a slope of 0.50 (within experimental error), and the fitting degree is very high ($R^2 = 0.9997$), which indicates that the interference of homoctopic elements in the mass spectrometry measurement process can be ignored. However, the $\delta^{26}\text{Mg}-\delta^{25}\text{Mg}$ diagrams of hydrothermal dolomite and calcite samples are distributed in different intervals (Figure 9B), indicating that there is mass fractionation between hydrothermal dolomite and calcite.

It is found that chondrites, mantle peridotites, and basalts have relatively homogeneous Mg isotopic compositions (Figure 10A) [61], suggesting that the mass balance fractionation of Mg isotopes is very small in processes of high-temperature magmatism, such as crystallization differentiation and partial melting [61,62]. In other words, the

Mg isotopic composition of carbonatites, which are genetically related to mantle-derived igneous rocks, should be similar to that of mantle-derived igneous rocks. For example, the $\delta^{26}\text{Mg}$ values of dolomite (igneous carbonatite dyke) in the Bayan Obo deposit range from -0.94‰ to -0.10‰ , with an average of -0.50‰ [63]; and the $\delta^{26}\text{Mg}$ values of the H8 dolomite range from -1.18‰ to 0.56‰ (average: -0.42‰) and are closely related to those of mantle rocks [64] (Figure 10B). In addition, some studies show that Mg isotopic compositions of different ages and types of sedimentary carbonate rocks have no obvious correlations beyond similar distribution intervals [24,64]. For example, ancient (Paleoproterozoic to Triassic) and modern (Cenozoic) dolostones have similar $\delta^{26}\text{Mg}$ compositions, ranging from -3.25‰ to -0.45‰ and -3.46‰ to -0.38‰ , respectively [26,39]. Therefore, carbonatites can be well distinguished from sedimentary carbonate rocks. The Mg isotopic compositions of hydrothermal carbonate rocks (dolomite and calcite) in the Lekai Pb-Zn deposit range from -3.853‰ to -1.358‰ , which are significantly lighter than those of chondrites, mantle rock, and seawater (Figure 10B), and close to those of sedimentary carbonate rocks. These data show that the source area of Mg in the metallogenic fluid of the Lekai Pb-Zn deposit may be sedimentary carbonate rocks, and has little relationship with mantle, sedimentary rock, or seawater.

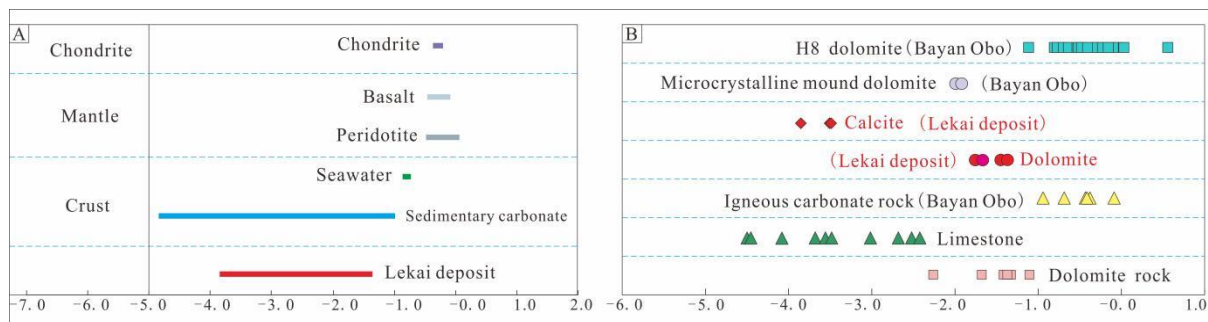


Figure 10. (A) Magnesium isotopic composition of different reservoirs of the Earth (Chondrite [13]; Mantle [34]; Crust [23,33]; (B) Magnesium isotopic composition of Lekai Pb-Zn deposit and Bayan Obo deposit (Bayan Obo deposit [63]).

The Mg isotopic compositions of hydrothermal dolomite and calcite in the Lekai Pb-Zn deposit are distributed in the sedimentary carbonate rocks interval. However, there is still a certain fraction (Figure 9B) wherein the average $\delta^{26}\text{Mg}$ value of hydrothermal dolomite is -1.548‰ , whereas that of calcite is -3.613‰ . It is found that Mg isotope fractionation of carbonate minerals is mainly affected by a combination of factors, including the following: the growth rate of carbonate minerals [28,65]; temperature [66]; the existing form of Mg in the aqueous solution [67]; biological processes [68,69]; and the type of carbonate minerals (different minerals have different Mg–O bond lengths) [23,36]. The REE characteristics of dolomite and calcite in the Lekai hydrothermal system show that they originated from the same fluid system, but the dolomite crystallized earlier than calcite, which indicates that the Mg isotopic fractionations of dolomite and calcite are not caused by the existence of Mg in the hydrothermal fluid. In addition, the Mg isotopic compositions of hydrothermal dolomite and calcite are relatively concentrated, suggesting that the influence of mineral growth rate is not significant. The biological effects first need to meet the temperature conditions for bacterial life and that of other organisms ($<100\text{--}120\text{ °C}$, [70]). The homogenization temperature of hydrothermal mineral fluid inclusions of Pb-Zn deposits in northwest Guizhou is between 160 °C and 260 °C [4]; therefore, the effect of biological action on Mg isotope fractionation can be eliminated. Some experimental and field data have shown that Mg isotopic fractionation during inorganic precipitation of carbonate minerals is positively correlated with the temperature at medium and low temperatures [43,66], but the influence of temperature on Mg isotopic fractionation is relatively weak, so it is not the main controlling factor [14,35,71]. However, this is not consistent with the fact that dolomite

with a little earlier crystallization should have a slightly heavier Mg isotopic composition than calcite $\delta^{26}\text{Mg}$. Mg isotopic fractionation is obviously beyond the influence range of temperature. Liu et al. (2010) [72] found that mineral phase is the main controlling factor of Mg isotopic fractionation in carbonate minerals, that is, the bond length or bond energy strength of the corresponding chemical bonds formed by Mg in different mineral phases determines the degree of Mg isotope fractionation. Generally, the bond length is determined by the coordination number of the cation (Mg), followed by the coordination number of the anion (generally O). The lower the coordination number, the shorter the bond length, and the stronger the bond energy, the more favorable it is for the enrichment of heavy Mg isotopes [14,72]. It is found that Mg–Ca substitution leads to strong deformation of the Mg ion lattice during dolomitization, resulting in the reduction of the coordination number and formation of stronger Mg–O bond energy. The concentrations of Mg and Ca in carbonate rocks also affect the Mg–O bond energy. The ratio of Mg to Ca in dolomite is more conducive to the enrichment of ^{26}Mg [73]. Therefore, dolomite has a heavier Mg isotopic composition than calcite. In addition, the relevant experimental data also show that carbonate minerals tend to be enriched in light Mg isotopes, and calcite has a greater fractionation coefficient than dolomite [14,36,66,74,75]. This is consistent with the results of this study. Therefore, we primarily think that the mineral phase controls the Mg isotope fractionation of dolomite and calcite in the Lekai Pb–Zn deposit.

5.3. Mineralization

Studies have confirmed that the mineralization of Pb–Zn deposits in the SYG Pb–Zn metallogenic province is a mixture of two kinds of fluids, such as acidic fluid rich in metal elements that originated from the basement is fed into the overlying sedimentary strata by deep faults and mixed with alkaline fluid rich in sulfate in the strata. As a result, thermochemical sulfate reduction (TSR) produces a large amount of S^{2-} , which combines with metal cations such as Pb^{2+} , Zn^{2+} , and Fe^{2+} in the metal fluid for mineralization [76] (Figure 11). The participation of basement fluid directly affects the scale and grade of the orebody. From west to east, the deep lithospheric Anninghe, Ganluo–Xiaojiang, and Yadu–Mangdong Faults are distributed in the SYG Pb–Zn metallogenic province. Our results show that the Pb–Zn deposits are distributed along these three faults in a lenticular linear manner. The Ganluo–Xiaojiang Fault in the central part has the highest mineralization intensity and the best continuity in the distribution of deposits, whereas the Anninghe and Yadu–Mangdong Faults on the west and east sides, respectively, are relatively inferior in mineralization intensity and scale.

The metallogenic belt of northeast Yunnan in the ore concentration area is mainly controlled by the Ganluo–Xiaojiang Fault, and the basement metamorphic rocks have developed in this area. The ore host strata of the Pb–Zn deposits are mainly Sinian, Devonian, and other older strata, which are greatly affected by the basement metallic fluid and form large-scale and high-grade Pb–Zn orebodies easily, such as the Huize, Maoping, and other super large Pb–Zn deposits and the Maozu, Fule, and other large Pb–Zn deposits. In particular, the amount of Pb + Zn in the Huize Pb–Zn deposit exceeds 5 million tons, and that in the Maoping Pb–Zn deposit exceeds 3 million tons [2,3]. However, the Pb–Zn deposits in the northwest Guizhou metallogenic belt are mainly controlled by the Yadu–Mangdong Fault at the eastern boundary of the SYG Pb–Zn metallogenic province. The basement metamorphic rocks are not developed. The ore host strata are mainly Carboniferous, Permian, and other strata, which are less affected by the metal-bearing fluids in the basement. It is not easy to form large-scale and high-grade Pb–Zn orebodies in this area. There are few metal elements, such as Ag, Ge, Cd, and Ga. The Lekai Pb–Zn deposit is located at the intersection of the northern part of the Yadu–Mangdong Fault and the secondary Luozehe Fault of the Xiaojiang Fault. The ore-bearing strata are Devonian carbonate rocks with good structural and lithological conditions. However, the deposit is small in scale and low grade. The main factor is that the basement fluid is not involved in the deposit, and the basement fluid is the main source area of metal elements.

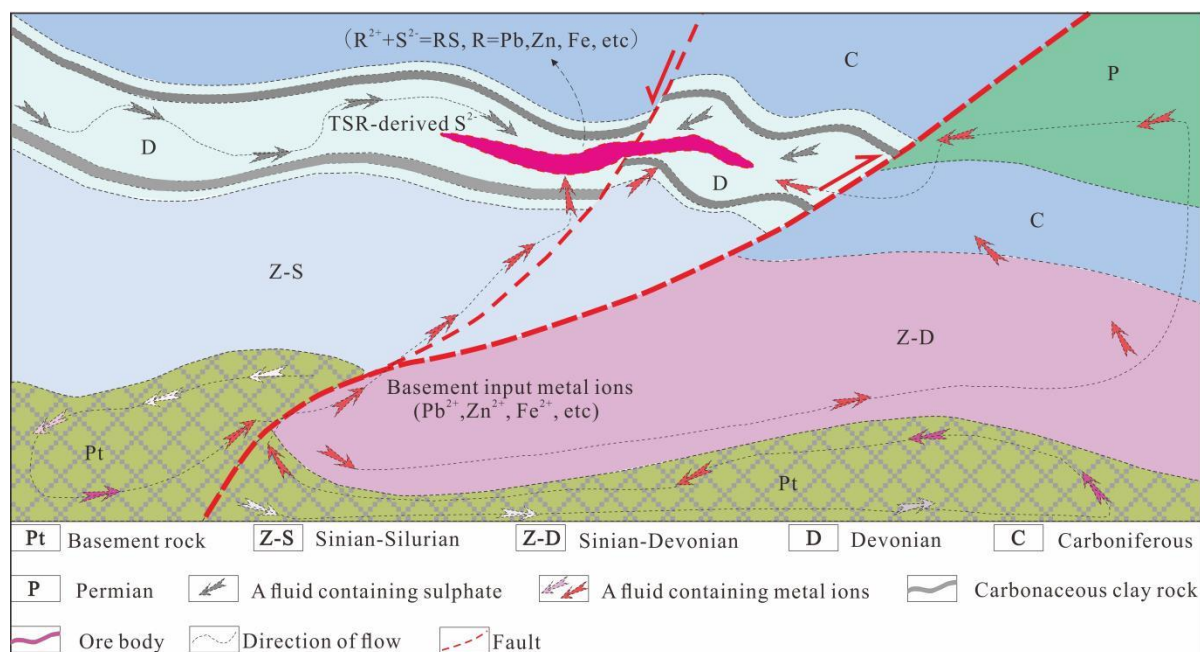


Figure 11. Metallogenic model map of Lekai Pb-Zn deposit [76].

6. Conclusions

Based on the in-depth analysis of the geological characteristics of the Lekai Pb-Zn deposit in the SYG Pb-Zn metallogenic province, and the systematic study of REE and C–O–Mg isotopic geochemistry of hydrothermal calcite/dolomite, the following four points are obtained:

- (I) The mineralization of the Lekai Pb-Zn deposit is mainly metasomatism and filling and controlled by faults and lithology. The orebody is stratoid and lenticular and develops veined, massive, brecciated, and disseminated structures, showing obvious epigenetic metallogenic characteristics.
- (II) The REE characteristics of hydrothermal calcite/dolomite in the Lekai Pb-Zn deposit show that the metallogenic materials are provided by the carbonate rocks, and the basin fluid is the main metallogenic fluid. The formation environment of the Pb-Zn deposit has low oxygen fugacity and low temperature. The C and O isotopic compositions of calcite/dolomite indicate that the metallogenic process is mainly influenced by the basement fluid, followed by basin fluid.
- (III) Mg isotopic analysis of hydrothermal calcite/dolomite in the Lekai Pb-Zn deposit shows that the source of metallogenic fluid may be sedimentary carbonate rocks, rather than the mantle, chondrites, or seawater. The Mg isotopic fractionation of calcite/dolomite is controlled by the mineral phase.
- (IV) The mineralization of Pb-Zn deposits in the SYG Pb-Zn metallogenic province may be the result of two fluids mixing (basement fluid and basin fluid). The participation of basement fluid directly affects the scale and grade of the orebody. The Lekai Pb-Zn deposit is obviously less affected by the basement fluid and shown small in deposit scale and grade.

Author Contributions: Conceptualization, Z.H. and B.L.; methodology, Z.H.; validation, Z.H., X.W. (Xinfu Wang) and X.X.; formal analysis, Z.H. and X.X. investigation, B.L. and X.W. (Xin Wan); data curation, Q.W.; writing—original draft preparation, Z.H.; writing—review and editing, Z.H., X.W. (Xinfu Wang) and B.L.; visualization, B.L. and X.W. (Xinfu Wang); supervision, B.L. and X.X.; funding acquisition, B.L. All authors have read and agreed to the published version of the manuscript.

Funding: This research was financially supported by the National Natural Science Foundation of China (No. 41862007), the Key Disciplines Construction of Kunming University of Science and

Technology (No. 14078384), and the Yunnan Ten Thousand Talents Plan Young & Elite Talents Project (No. YNWR-QNBJ-2018-093).

Data Availability Statement: The data used to support this study are included within the article.

Acknowledgments: We sincerely thank the Editorial Board members and anonymous reviewers for their constructive comments.

Conflicts of Interest: The authors declare that they have no known competing financial interest or personal relationships that could have appeared to influence the work reported in this paper.

References

1. Hu, R.Z.; Fu, S.; Huang, Y.; Zhou, M.; Fu, S.; Zhao, C.; Wang, Y.; Bi, X.; Xiao, J. The giant South China Mesozoic low-temperature metallogenic province: Reviews and a new geodynamic model. *J. Asian Earth Sci.* **2017**, *137*, 9–34. [[CrossRef](#)]
2. Han, R.S.; Zou, H.J.; Hu, B.; Hu, Y.Z.; Xue, C.D. Features of fluid inclusions and sources of ore-forming fluid in the Maoping carbonate-hosted Zn-Pb-(Ag-Ge) deposit, Yunnan, China. *Acta Petrol. Sin.* **2007**, *23*, 2109–2118.
3. Han, R.S.; Hu, Y.Z.; Wang, X.K.; Hou, B.H.; Huang, Z.L.; Chen, J.; Wang, F.; Wu, P.; Li, B.; Wang, H.J.; et al. Mineralization model of rich Ge-Ag-bearing Zn-Pb polymetallic deposit concentrated district in Northeastern Yunnan, China. *Acta Geol. Sin. Ed.* **2012**, *86*, 280–294.
4. Zhu, L.Y.; Su, W.C.; Shen, N.P.; Dong, W.D.; Cai, J.L.; Zhang, Z.W.; Zhao, H.; Xie, P. Fluid inclusion and sulfur isotopic northwestern Guizhou, China. *Acta Petrol. Sin.* **2016**, *32*, 3431–3440.
5. Yuan, B.; Mao, J.W.; Yan, X.H.; Wu, Y.; Zhang, F.; Zhao, L.L. Sources of metallogenic materials and metallogenic mechanism of Daliangzi Ore Field in Sichuan Province: Constraints from geochemistry of S, C, H, O, Sr isotope and trace element in sphalerite. *Acta Petrol. Sin.* **2014**, *30*, 209–220.
6. Qiu, W.L.; Han, R.S. Study on hydrogen and oxygen isotopic characteristics of Zhaotong lead-zinc deposit. *Acta Geol. Sin.* **2015**, *89*, 173–174.
7. Zhou, J.X.; Huang, Z.L.; Zhou, M.; Li, X.; Jin, Z. Constraints of C-O-S-Pb isotope compositions and Rb-Sr isotopic age on the origin of the Tianqiao carbonate-hosted Pb-Zn deposit, southwest China. *Ore Geol. Rev.* **2013**, *53*, 77–92. [[CrossRef](#)]
8. Zhou, J.X.; Huang, Z.L.; Bao, G. Geological and sulfur-lead-strontium isotopic studies of the Shaojiwan Pb-Zn deposit, southwest China: Implications for the origin of hydrothermal fluids. *J. Geochemical. Explor.* **2013**, *128*, 51–61. [[CrossRef](#)]
9. Zhou, J.X.; Huang, Z.L.; Gao, J.G.; Yan, Z.F. Geological and C-O-S-Pb-Sr isotopic constraints on the origin of the Qingshan carbonate-hosted Pb-Zn deposit, Southwest China. *Ore Geol. Rev.* **2013**, *55*, 904–916. [[CrossRef](#)]
10. Zhou, J.X.; Huang, Z.L.; Bao, G.; Gao, J.G. Sources and thermo-chemical sulfate reduction for reduced sulfur in the hydrothermal fluids, southeastern SYG Pb-Zn metallogenic province, southwest China. *J. Asian Earth Sci.* **2013**, *24*, 759–771.
11. Ye, L.; Gao, W.; Yang, Y.L.; Liu, T.G.; Peng, S.S. Trace elements in sphalerite in Laochang Pb-Zn polymetallic deposit, Lancang, Yunnan Province. *Acta Petrologica. Sin.* **2012**, *28*, 1362–1372.
12. Zhou, J.X.; Luo, K.; Wang, X.C.; Simon, A.W.; Wu, T.; Huang, Z.L.; Cui, Y.L.; Zhao, X.Z. Ore genesis of the Fule Pb-Zn deposit and its relationship with the Emeishan Large Igneous Province: Evidence from mineralogy, bulk C-O-S and in situ S-Pb isotopes. *Gondwana Res.* **2018**, *54*, 161–179. [[CrossRef](#)]
13. Galy, A.; Young, E.D.; Ash, R.D.; O’Nions, R.K. The formation of chondrules at high gas pressures in the solar nebula. *Science* **2000**, *290*, 1751–1753. [[CrossRef](#)] [[PubMed](#)]
14. Galy, A.; Matthews, M.B.; Halicz, L.; O’Nions, R.K. Mg isotopic composition of carbonate: Insight from speleothem formation. *Earth Planet. Sci. Lett.* **2002**, *201*, 105–110. [[CrossRef](#)]
15. Galy, A.; Yoffe, O.; Janney, P.E.; Williams, R.W.; Cloquet, C.; Alard, O.; Halicz, L.; Wadhwa, M.; Hutcheon, I.D.; Ramon, E.; et al. Magnesium isotope heterogeneity of the isotopic standard SRM980 and new reference materials for magnesium-isotope-ratio measurements. *J. Anal. At. Spectrom.* **2003**, *18*, 1352–1356. [[CrossRef](#)]
16. Wilkinson, J.J.; Weiss, D.J.; Mason, T.F.D.; Coles, B.J. zinc isotope variation in hydrothermal systems: Preliminary evidence from the Irish Midlands ore field. *Economic. Geology* **2005**, *100*, 583–590. [[CrossRef](#)]
17. Fujii, T.; Moynier, F.; Pons, M.L.; Albarède, F. The origin of Zn isotope fractionation in sulfides. *Geochim. Cosmochim. Acta* **2011**, *75*, 7632–7643. [[CrossRef](#)]
18. Tang, S.H.; Zhu, X.K.; Li, J.; Yan, B.; Li, S.Z.; Li, Z.H.; Wang, Y.; Sun, J. New Standard Solutions for Measurement of Iron, Copper and zinc Isotopic Compositions by Multi-collector Inductively Coupled Plasma-Mass Spectrometry. *Rock Miner. Anal.* **2016**, *35*, 127–133.
19. Duan, J.; Tang, J.; Lin, B. zinc and lead isotope signatures of the Zhaxikang Pb-Zn deposit, South Tibet: Implications for the source of the mineralizing metals. *Ore Geol. Rev.* **2016**, *78*, 58–68. [[CrossRef](#)]
20. Gagnevin, D.; Boyce, A.J.; Barrie, C.D.; Menuge, J.F.; Blakeman, R.J. Zn, Fe and S isotope fractionation in a large hydrothermal system. *Geochim. Cosmochim. Acta* **2012**, *88*, 183–198. [[CrossRef](#)]
21. Zhou, J.X.; Xiang, Z.Z.; Zhou, M.F.; Feng, Y.X.; Luo, K.; Huang, Z.L.; Wu, T. The giant Upper Yangtze Pb-Zn province in southwest China: Reviews, new advances and a new genetic model. *J. Asian Earth Sci.* **2018**, *154*, 280–315. [[CrossRef](#)]
22. Galy, A.; Belshaw, N.S.; Halicz, L.; O’Nions, R.K. High-Precision measurement of magnesium isotopes by multiples collector inductively coupled plasma mass spectrometry. *Int. J. Mass Spectrom.* **2001**, *208*, 89–98. [[CrossRef](#)]

23. Young, E.D.; Galy, A. The isotope geochemistry and cosmochemistry of magnesium. *Rev. Mineral. Geochem.* **2004**, *55*, 197–230. [[CrossRef](#)]
24. Ge, L.; Jiang, S.Y. Recent advances in research on magnesium isotope geochemistry. *Acta Petrol. Mineral.* **2008**, *27*, 367–374.
25. Ke, S.; Liu, S.A.; Li, W.H.; Yang, W.; Teng, F.Z. Advances and application in magnesium isotope geochemistry. *Acta Petrol. Sin.* **2011**, *27*, 383–397.
26. Teng, F.Z. Magnesium isotope geochemistry. *Rev. Mineral. Geochem.* **2017**, *82*, 219–287. [[CrossRef](#)]
27. Azmy, K.; Lavoie, D.; Wang, Z.R.; Brand, U.; Al-Aasm, I.; Jackson, S.; Girard, I. Magnesium-isotope and REE compositions of Lower Ordovician carbonates from eastern Laurentia: Implications for the origin of dolomites and limestones. *Chem. Geol.* **2013**, *356*, 64–75. [[CrossRef](#)]
28. Mavromatis, V.; Meister, P.; Oelkers, E.H. Using stable Mg isotopes to distinguish dolomite formation mechanisms: A case study from the Peru Margin. *Chem. Geol.* **2014**, *385*, 84–91. [[CrossRef](#)]
29. Geske, A.; Goldstein, R.H.; Mavromatis, V.; Richter, D.K.; Buhl, D.; Kluge, T.; John, C.M.; Immenhauser, A. The magnesium isotope ($\delta^{26}\text{Mg}$) signature of dolomites. *Geochim. Cosmochimica Acta* **2015**, *149*, 131–151. [[CrossRef](#)]
30. Wan, X.; Han, R.S.; Li, B.; Xiao, X.G.; He, Z.W.; Wang, J.T.; Wei, Q.X. Tectono-geochemistry and deep prospecting prediction in the Lekai lead-zinc deposit, NW Guizhou Province, China. *Geol. China* **2020**. Available online: <http://kns.cnki.net/kcms/detail/11.1167.P20200602.1143.011.html> (accessed on 2 June 2020).
31. Young, E.D.; Galy, A.; Nagahara, H. Kinetic and equilibrium mass-dependent isotope fractionation laws in nature and their geochemical and cosmochemical significance. *Geochim. Cosmochim. Acta* **2002**, *66*, 1095–1104. [[CrossRef](#)]
32. Young, E.D.; Tonui, E.; Manning, C.E.; Schauble, E.; Macris, C.A. Spinel-olivine magnesium isotope thermometry in the mantle and implications for the Mg isotopic composition of Earth. *Earth Planet. Sci. Lett.* **2009**, *288*, 524–533. [[CrossRef](#)]
33. Chang, V.T.C.; Makishima, A.; Belshaw, N.S.; Keith O’Nions, R. Purification of Mg from low-Mg biogenic carbonates for isotope ratio determination using multiple collector ICP-MS. *J. Anal. At. Spectrom.* **2003**, *18*, 296–301. [[CrossRef](#)]
34. Pearson, N.J.; Griffin, W.L.; Alard, O.; O’Reilly, S.Y. The isotopic composition of magnesium in mantle olivine: Records of depletion and metasomatism. *Chem. Geol.* **2006**, *226*, 115–133. [[CrossRef](#)]
35. Immenhauser, A.; Bauhl, D.; Richter, D.; Niedermayr, A.; Riechelmann, D.; Dietzel, M.; Schulte, U. Magnesium-isotope fractionation during low-Mg calcite precipitation in a limestone cave-Field study and experiments. *Geochim. Cosmochim. Acta* **2010**, *74*, 4346–4364. [[CrossRef](#)]
36. Wang, Z.R.; Hu, P.; Gaetani, G.; Liu, C.; Saenger, C.; Cohen, A.; Hart, S. Experimental calibration of Mg isotope fractionation between aragonite and seawater. *Geochim. Cosmochim. Acta* **2013**, *102*, 113–123. [[CrossRef](#)]
37. Lavoie, D.; Jackson, S.; Girard, I. Magnesium isotopes in high-temperature saddle dolomite cements in the lower Paleozoic of Canada. *Sediment. Geol.* **2014**, *305*, 58–68. [[CrossRef](#)]
38. Yoshimura, T.; Tanimizu, M.; Inoue, M.; Inoue, M.; Suzuki, A.; Iwasaki, N.; Kawahata, H. Mg isotope fractionation in biogenic carbonates of deep-sea coral, benthic foraminifera, and hermatypic coral. *Anal. Bioanal. Chem.* **2011**, *401*, 2755–2769. [[CrossRef](#)]
39. Huang, K.J.; Shen, B.; Lang, X.G.; Tang, W.; Peng, Y.; Ke, S.; Kaufman, A.; Ma, H.R.; Li, F.B. Magnesium isotopic composition of the Mesoproterozoic dolostones: Implications for Mg isotopic systematics of marine carbonates. *Geochim. Cosmochimica Acta* **2015**, *614*, 333–351. [[CrossRef](#)]
40. Guan, S.P.; Li, Z.X. Lead-sulfur isotope study of carbonate-hosted Pb-Zn deposits at the eastern margin of the kangdian axis. *Geol. Geochem.* **1999**, *27*, 45–54.
41. Zhang, C.Q.; Wu, Y.; Hou, L.; Mao, J.W. Geodynamic setting of mineralization of Mississippi Valley-type deposits in world-class SYG Zn-Pb triangle, southwest China: Implications from age-dating studies in the past decade and the Sm-Nd age of the Jinshachang deposit. *J. Asian Earth Sci.* **2015**, *103*, 103–114. [[CrossRef](#)]
42. Schwinn, G.; Markl, G. REE systematics in hydrothermal fluorite. *Chem. Geol.* **2005**, *216*, 225–248. [[CrossRef](#)]
43. Li, W.; Chakraborty, S.; Beard, B.L.; Romanek, C.S.; Johnson, C.M. Magnesium isotope fractionation during precipitation of inorganic calcite under laboratory conditions. *Earth Planet. Sci. Lett.* **2012**, *333*, 304–316. [[CrossRef](#)]
44. Bau, M.; Dulski, P. Comparative study of yttrium and rare-earth element behavior in fluorine-rich hydrothermal fluids. *Contrib. Mineral. Petrol.* **1995**, *119*, 213–223. [[CrossRef](#)]
45. Möller, P.; Parekh, P.P.; Schneider, H.J. The application of Tb/Ca–Tb/La abundance ratios to problems of fluorspar genesis. *Miner. Depos.* **1976**, *11*, 111–116. [[CrossRef](#)]
46. Michard, A. Rare earth element systematics in hydrothermal fluids. *Geochim. Cosmochim. Acta* **1989**, *53*, 745–750. [[CrossRef](#)]
47. Bau, M.; Möller, P. Rare earth element fractionation in metamorphogenic hydrothermal calcite, magnesite and siderite. *Miner. Petrol.* **1992**, *45*, 231–246. [[CrossRef](#)]
48. Bau, M. Rare-earth element mobility during hydrothermal and metamorphic fluid-rock interaction and the significance of the oxidation state of europium. *Chem. Geol.* **1991**, *93*, 219–230. [[CrossRef](#)]
49. Subías, I.; Fernández-Nieto, C. Hydrothermal events in the Valle de Tena (Spanish Western Pyrenees) as evidenced by fluid inclusions and trace-element distribution from fluorite deposits. *Chem. Geol.* **1995**, *124*, 267–282. [[CrossRef](#)]
50. Constantopoulos, J. Fluid inclusions and rare-earth element geochemistry of fluorite from south-central Idaho. *Econ. Geol.* **1988**, *88*, 626. [[CrossRef](#)]
51. Chesley, J.T.; Halliday, A.N.; Scrivener, R.C. Samarium-Neodymium Direct of Fluorite. *Science* **1991**, *252*, 949–951. [[CrossRef](#)] [[PubMed](#)]

52. Xu, C.; Taylor, R.N.; Li, W.; Kynicky, J.; Chakhmouradian, A.R.; Song, W. Comparison of fluorite geochemistry from REE deposits in the Panxi region and Bayan Obo, China. *J. South. Hemisph. Earth Syst. Sci.* **2012**, *57*, 76–89. [[CrossRef](#)]
53. Pei, Q.M.; Zhang, S.T.; Santosh, M.; Cao, H.W.; Zhang, W.; Hu, X.K.; Wang, L. Geochronology, geochemistry, fluid inclusion and C, O and Hf isotope compositions of the Shuitou fluorite deposit, Inner Mongolia, China. *Ore Geol. Rev.* **2017**, *83*, 174–190. [[CrossRef](#)]
54. Möller, P.; Morteani, G. On the chemical fractionation of REE during the formation of Ca-minerals and its application to problems of the genesis of ore deposits. In *The Significance of Trace Elements in Solving Petrogenetic Problems*; Augustithis, S., Ed.; Theophrastus Publications: Athens, Greece, 1983; pp. 747–791.
55. Liu, J.M.; Liu, J.J. Basin fluid genetic model of sediment-hosted micro-disseminated gold deposits in the gold-triangle area between Guizhou, Guangxi and Yunnan. *Acta Mineral. Sin.* **1997**, *17*, 448–456.
56. Taylor, H.P.; Frechen, J.; Degens, E.T. Oxygen and carbon isotope studies of carbonatites from the Laacher See District, West Germany and the Alnö District, southweden. *Geochim. Cosmochim. Acta* **1967**, *31*, 407–430. [[CrossRef](#)]
57. Hoefs, J. *Stable Isotope Geochemistry*, 4th ed.; Springer: Berlin, Germany, 1997; pp. 65–168.
58. Veizer, J.; Hoefs, J. The nature of O18/O16 and C13/C12 secular trends in sedimentary carbonate rocks. *Geochim. Et Cosmochim. Acta* **1976**, *40*, 1387–1395. [[CrossRef](#)]
59. Zhou, J.X.; Huang, Z.L.; Lv, Z.C.; Zhu, X.K.; Gao, J.G.; Mirnejad, H. Geology, isotope geochemistry and ore genesis of the Shanshulin carbonate-hosted Pb-Zn deposit, southwest China. *Ore Geol. Rev.* **2014**, *63*, 209–225. [[CrossRef](#)]
60. He, Z.W.; Li, Z.Q.; Li, B.; Chen, J.; Xiang, Z.P.; Wang, X.F.; Du, L.J.; Huang, Z.L. Ore genesis of the Yadu carbonate-hosted Pb-Zn deposit in Southwest China: Evidence from rare earth elements and C, O, S, Pb, and Zn isotopes. *Ore Geol. Rev.* **2021**, *131*, 104039. [[CrossRef](#)]
61. Teng, F.Z.; Li, W.Y.; Ke, S.; Marty, B.; Dauphas, N.; Huang, S.C.; Wu, F.Y.; Pourmand, A. Magnesium isotopic composition of the Earth and chondrites. *Geochim. Cosmochim. Acta* **2010**, *74*, 4150–4166. [[CrossRef](#)]
62. Teng, F.Z.; Wadhwa, M.; Helz, R.T. Investigation of magnesium isotope fractionation during basalt differentiation: Implications for a chondritic composition of the terrestrial mantle. *Earth Planet. Sci. Lett.* **2007**, *261*, 84–92. [[CrossRef](#)]
63. Sun, J. *The Origin of the Bayan Obo Ore Deposit, Inner Mongolia, China: The Iron and Magnesium Isotope Constraints*; China University of Geosciences: Beijing, China, 2013; pp. 1–115.
64. Ning, M.; Huang, K.J.; Shen, B. Applications and advances of the magnesium isotope on the ‘dolomite problem’. *Acta Petrol. Sin.* **2018**, *34*, 3690–3708.
65. Mavromatis, V.; Gautier, Q.; Bosc, O.; Schott, J. Kinetics of Mg partition and Mg stable isotope fractionation during its incorporation in calcite. *Geochim. Cosmochim. Acta* **2013**, *114*, 188–203. [[CrossRef](#)]
66. Li, W.Q.; Beard, B.L.; Li, C.X.; Xu, H.F.; Johnson, C.M. Experimental calibration of Mg isotope fractionation between dolomite and aqueous solution and its geological implications. *Geochim. Et Cosmochim. Acta* **2015**, *157*, 164–181. [[CrossRef](#)]
67. Schott, J.; Mavromatis, V.; Fujii, T.; Pearce, C.R.; Oelkers, E.H. The control of carbonate mineral Mg isotope composition by aqueous speciation: Theoretical and experimental modeling. *Chem. Geol.* **2016**, *445*, 120–134. [[CrossRef](#)]
68. Pogge von Strandmann, P.A.E.; Burton, K.W.; James, R.H.; Calsteren, P.; Gislason, S.R.; Sigfússon, B. The influence of weathering processes on riverine magnesium isotopes in a basaltic terrain. *Earth Planet. Sci. Lett.* **2008**, *276*, 187–197. [[CrossRef](#)]
69. Hippler, D.; Buhl, D.; Witbaard, R.; Richter, D.K.; Immenhauser, A. Towards a better understanding of magnesium-isotope ratios from marine skeletal carbonates. *Geochim. Cosmochim. Acta* **2009**, *73*, 6134–6146. [[CrossRef](#)]
70. Basuki, N.I.; Taylor, B.E.; Spooner, E.T.C. Sulfur isotope evidence for thermo-chemical reduction of dissolved sulfate in Mississippi valley type zinc-lead mineralization, Bongara area, northern Peru. *Economic. Geol.* **2008**, *103*, 183–799. [[CrossRef](#)]
71. Tang, B.; Wang, J.T.; Fu, Y. Magnesium Isotope Composition of Different Geological Reservoirs and Controlling Factors of Magnesium Isotope Fractionation in the Formation of Carbonate Minerals-A Summary of Previous Results. *Rock Miner. Anal.* **2020**, *39*, 162–173.
72. Liu, S.A.; Teng, F.Z.; He, Y.S.; Ke, S.; Li, S.G. Investigation of magnesium isotope fractionation during granite differentiation: Implication for Mg isotopic composition of the continental crust. *Earth Planet. Sci. Lett.* **2010**, *297*, 646–654. [[CrossRef](#)]
73. Pinilla, C.; Blanchard, M.; Balan, E.; Natarajan, S.K.; Vuilleumier, R.; Mauri, F. Equilibrium magnesium isotope fractionation between aqueous Mg²⁺ and carbonate minerals: Insights from path integral molecular dynamics. *Geochim. Cosmochim. Acta* **2015**, *163*, 126–139. [[CrossRef](#)]
74. Saulnier, S.; Rollion-Bard, C.; Vigier, N.; Chaussidon, M. Mg isotope fractionation during calcite precipitation: An experimental study. *Geochim. Cosmochim. Acta* **2012**, *91*, 75–91. [[CrossRef](#)]
75. Mavromatis, V.; Pearce, C.R.; Shirokova, L.S.; Bundelava, I.A.; Pokrovsky, O.S.; Benezeth, P.; Oelkers, E.H. Magnesium isotope fractionation during hydrous magnesium carbonate precipitation with and without cyanobacteria. *Geochim. Cosmochim. Acta* **2012**, *76*, 161–174. [[CrossRef](#)]
76. Xiao, X.G.; Li, B.; He, Z.W.; Wang, J.T.; Wei, Q.X.; Wan, X. Sources of metallogenic materials and genesis of Lekai lead-zinc deposit in northwestern Guizhou Province: Evidence from S and Pb isotopes. *Miner. Depos.* **2022**, *41*, 806–822. (In Chinese with English Abstract)